Arabian Journal of Chemistry (2015) 8, 553–559

King Saud University

Arabian Journal of Chemistry

www.ksu.edu.sa
www.sciencedirect.com

ORIGINAL ARTICLE

ZnO nanostructures induced by microwave plasma

Khaled A. Elsayed [a,c,*], Noori S. Anad [a], Gamal AbdelFattah [b], Hisham Imam [b], Tarek S. Kayed [c], Lotfi Z. Ismail [a]

[a] Department of Physics, Faculty of Science, Cairo University, Egypt
[b] National Institute of Laser Enhanced Science (NILES), Cairo University, Egypt
[c] College of Engineering, University of Dammam, Dammam, Kingdom of Saudi Arabia

Received 17 May 2014; accepted 24 November 2014
Available online 2 December 2014

KEYWORDS

ZnO nanostructure;
Nanorods;
Band gap

Abstract Microwave induced hydrogen plasma is used to fabricate ZnO thin films at low ambient gas pressure and controlled oxygen content in the gas mixture. The emission spectra have been observed. Optical emission spectroscopy was used to identify the chemical reaction mechanism. Structural quality of the so-obtained nanoparticles was studied by X-ray diffraction (XRD) and high resolution scanning electron microscopy (SEM). SEM results showed that nanorods were formed in the process, and XRD results along with nanorod dimensions obtained from SEM are consistent with the formation of single and poly-crystalline ZnO nanorods. The alignment of these nanorods with respect to the substrates depends on the lattice mismatch between ZnO and the glass substrate. The minimum crystallite grain size as obtained from the SEM measurements was ~24 nm and the average diameter is 70 nm with a length of 1–2 μm. The deposited ZnO thin films have a wide energy band gap that equals ~3 eV.

1. Introduction

Oxide materials, especially zinc oxide (ZnO), attracted increasing attention of the researchers in the last few years because of their unique optical and transport properties. ZnO has a great potential for many optoelectronic applications due to its wide band gap (3.37 eV) and large exciton binding energy (60 meV) at room temperature (Yang et al., 2011; Ono and Iizuka, 2011; Irzh et al., 2010; Ismail et al., 2002). Different methods have been used to fabricate various ZnO nanostructures in the form of thin films (Yang et al., 2011; Ono and Iizuka, 2011; Irzh et al., 2010; Ismail et al., 2002; Craciun et al., 1995; Gao and Wang, 2002; Chang et al., 2004; Singh et al., 2008; Bashir et al., 2009; Masuda and Kato, 2009; Ashida et al., 2008). Chemical vapor deposition method (CVD) is widely used in materials-processing technology but it usually works at a high temperature, which is considered as a main disadvantage of the fabrication process. Metal Organic Chemical Vapor Phase Deposition (MOCVD) is a highly complex process for growing crystalline layers that was developed to overcome the above-mentioned problem (Ismail et al., 2002). There are many other techniques that are used to synthesize ZnO thin films,

* Corresponding author at: Department of Physics, Faculty of Science, Cairo University, Egypt.
Peer review under responsibility of King Saud University.

Production and hosting by Elsevier

http://dx.doi.org/10.1016/j.arabjc.2014.11.035
1878-5352

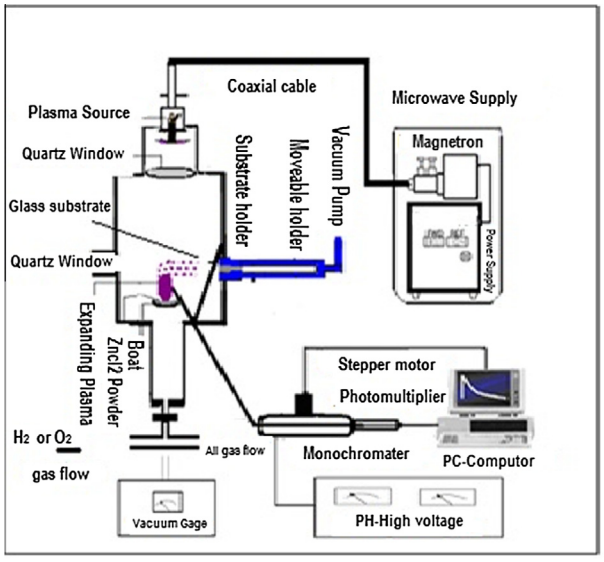

Figure 1 Low pressure microwave plasma-chemical vapor deposition (LPMP CVD) setup.

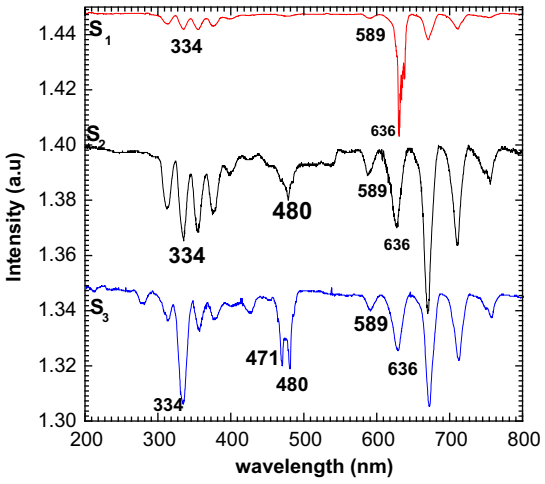

Figure 3 Typical plasma optical spectrum for three different samples prepared at three different gas mixtures of hydrogen and argon partial gas pressure ratio (3:1), (5:2), and (6:2) for samples S_1, S_2, and S_3, respectively.

Table 1 Preparation conditions of the three samples. The process voltage and the deposition time were 700 V and 30 min respectively for the all samples.

Sample	Hydrogen gas pressure (Torr)	Argon gas pressure (Torr)	Total pressure (Torr)	Microwave power (W)
S_1	3	1	4	250
S_2	5	2	7	300
S_3	6	2	8	300

including Pulsed Laser Deposition (PLD) (Craciun et al., 1995), reactive thermal vacuum evaporation (Gao and Wang, 2002), chemical vapor deposition (Chang et al., 2004), reactive magnetic sputtering (Singh et al., 2008), spray pyrolysis (Bashir et al., 2009), sol–gel techniques (Masuda and Kato, 2009) and electrochemical deposition (Ashida et al., 2008). The most common methods used for chemical vapor deposition are those applying radiofrequency and microwave techniques. The microwave method has proven to be better than the radio frequency method due to its plasma stability, symmetry, and sensitivity of oxidation process crystallization (Ismail et al., 2002).

The physical properties of the prepared thin films depend on microwave guide and geometry inside the reaction chamber with respect to the microwave modes. The oxidation contents are also dependent on the microwave modes and the plasma stability (Ismail et al., 2003). The physical properties such as energy gap and band structure can be extracted from the optical characterization of the thin films (Caglar et al., 2006). Two

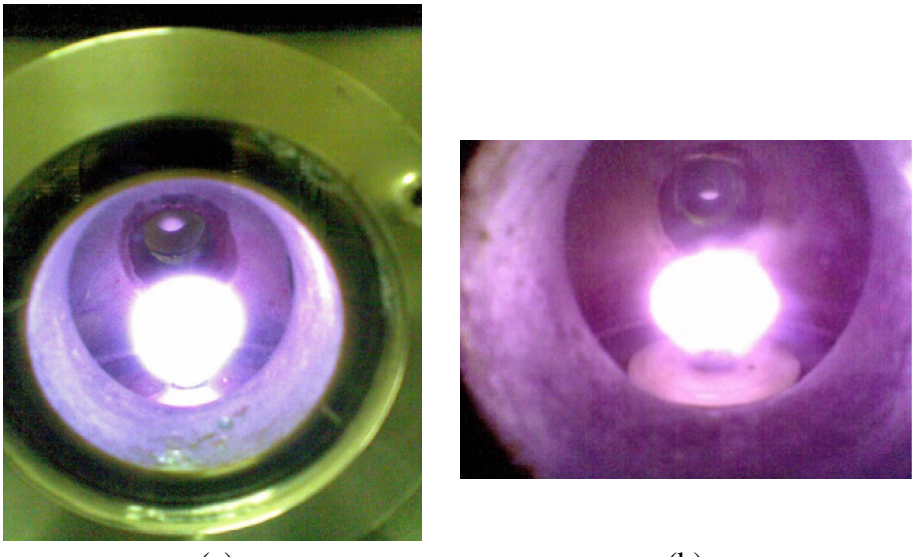

(a) (b)

Figure 2 Induced hydrogen plasma photograph taken during deposition (a) at applied power of 100 W, (b) at applied power of 300 W.

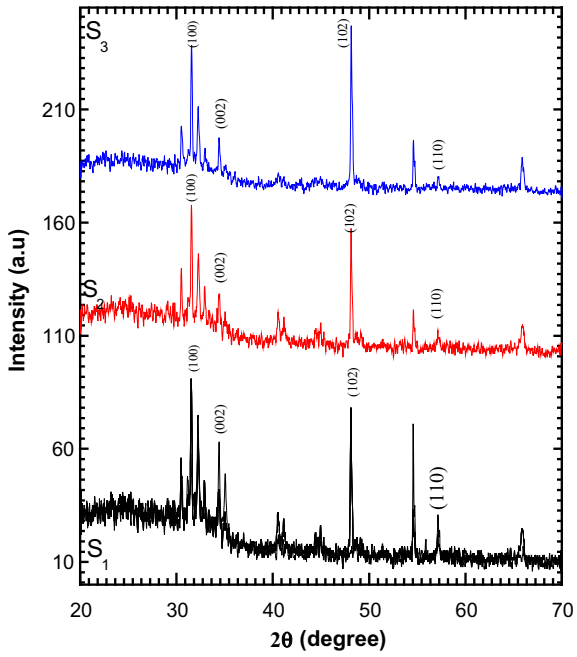

Figure 4 XRD patterns of the ZnO thin films for three samples prepared at three different gas mixture ratios of hydrogen and argon. The partial gas pressure ratios were (3:1) Torr for S_1, (5:2) Torr for S_2, and (6:2) Torr for S_3.

crystal structures can be obtained when synthesizing thin films depending on the preparation method used. The most common structure was hexagonal (Ono and Iizuka, 2011; Irzh et al., 2010; Zhang et al., 2004; Newton and Warburton, 2007; Tang et al., 2008; Yang et al., 2009).

In this paper, ZnO thin film is synthesized from $ZnCl_2$ powder using microwave longitudinal mode at low gas pressure. The presence of Zn and ZnO in the excited plasma has been observed in situ. The structure of the deposited thin film by plasma enhanced chemical vapor deposition (PECVD) technique which was used to obtain ZnO nanostructures at low temperatures by the oxidation of $ZnCl_2$ with a mixture of hydrogen and argon gas. X-ray diffraction (XRD) and scanning electron microscope (SEM) have been used to study the crystal structure of the deposited thin film synthesized by microwave plasma and its grain size. The optical properties of the fabricated thin film have also been investigated.

2. Experimental

The plasma CVD system used in this study is shown in Fig. 1. The plasma system consists of microwave generator operating at 2.45 GHz and magnetron (Toshiba 2M172H AG) that was connected through a 50-Ω cable with a radiator at the center of the cylindrical waveguide. The diameter and the length were 9.6 and 12 cm, respectively. The guided radiation power was fed into the plasma stainless-steel chamber (diameter = 10 cm; length = 6 cm). A Zinc Chloride powder ($ZnCl_2$) was sited in molybdenum (Mo) boat inside the center of the chamber. The substrate–target position was at angle 45° to the chamber wall inside the waveguide. The plasma spectra were collected during the deposition by an optical system into optical spectrometer (H20 monochromator from HORBIA, Jobin–Yvon).

The chamber was evacuated using a rotary pump (CIT) from Alcatel (2002B) and then subsequently argon and hydrogen gases were introduced into the chamber at different ratios. The applied microwave power was varied from 50 to 450 W. Measurements of plasma spectra were performed in the pressure range of 2–18 Torr. The plasma temperature was estimated to be 7 eV (Ismail and EL-Magd, 1992). Plasma reaction is totally isolated from the chamber walls as shown in Fig. 2.

The deposition time was set to be 30 min for each process. After that time, the microwave plasma power was switched off and H_2 flow was cut off then the system was left for 15 min to cool down to room temperature with a gas flow of argon at 3 Torr. The ZnO thin film was deposited on the upper side

Table 2 The grain size is calculated using 2θ, d-value and the full width at half maximum (FWHM) of zinc oxide nanoparticles for samples S_1, S_2 and S_3. hkl are the Miller indices for the observed diffraction plans.

(hkl)	Pos. [2θ]	Height [cts]	FWHM [2θ]	d-spacing (Å)	Rel. int. [%]	Grain size (nm)
(a) S_1						
(100)	31.51	12.47	0.1574	2.838	39.61	53
(002)	34.39	17.50	0.0984	2.607	55.57	86
(102)	47.90	3.87	0.1968	2.018	12.27	44
(110)	57.20	6.82	0.1574	1.610	21.65	58
Average grain size						60
(b) S_2						
(100)	31.533	81.09	0.138	2.8373	100.00	60
(002)	34.414	31.79	0.118	2.6061	39.20	70
(102)	48.095	69.06	0.118	1.8919	85.16	74
(110)	57.166	9.10	0.236	1.6114	11.23	38
Average grain size						61
(c) S_3						
(100)	31.54	34.31	0.0984	2.836	2.34	85
(002)	34.35	6.05	0.4723	2.610	0.41	18
(102)	48.09	27.85	0.0787	1.892	1.90	113
(110)	57.59	3.00	0.0984	1.600	0.20	94
Average grain size						78

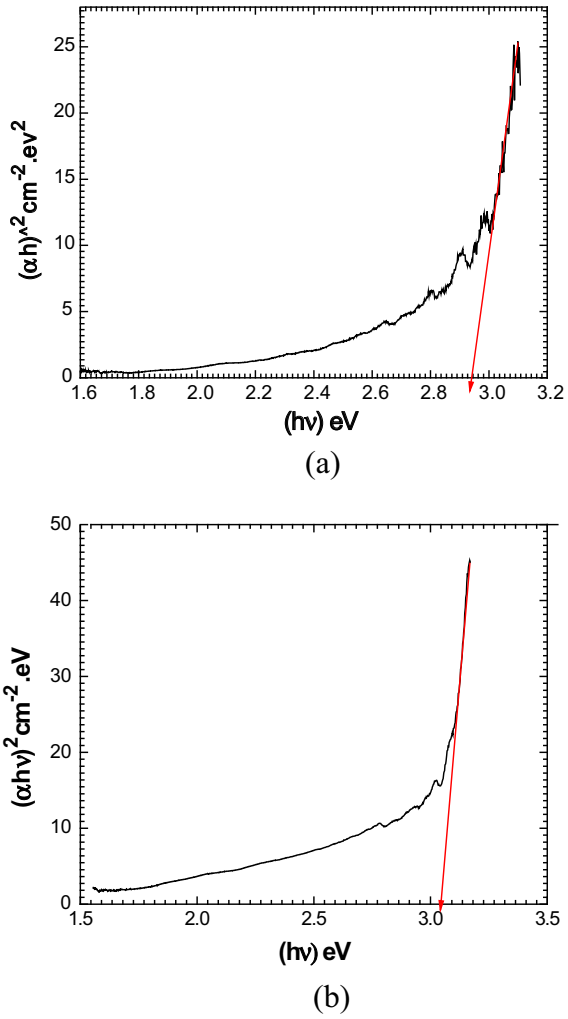

Figure 5 Measurement of energy gap for ZnO thin film prepared with partial gas pressure ratio for hydrogen and argon (a) (3:1) and (b) (5:2).

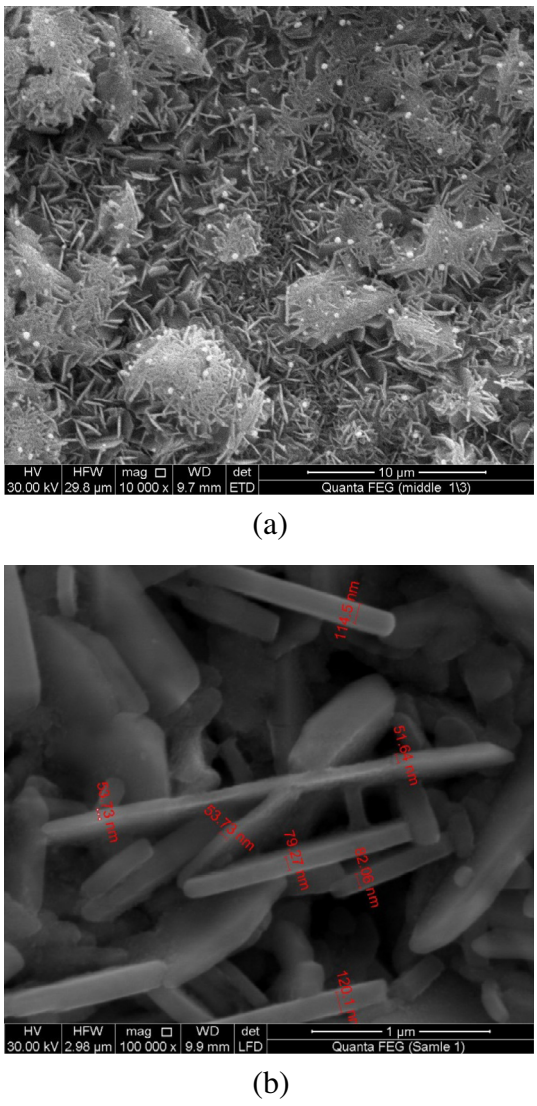

Figure 6 SEM images of the ZnO nanostructure (a) partial gas pressure ratio of hydrogen and argon is (5:2), (b) partial gas pressure ratio of hydrogen and argon is (3:1).

of the glass substrate at different ratios of hydrogen and argon gas pressures. The preparation conditions of the three samples are shown in Table 1.

3. Results and discussion

Fig. 3 shows the emission spectra of plasma at the three different gas ratios mentioned above. The spectra consisted of strong emission lines of neutral zinc (Zn) observed at 334 nm, 471 nm, and 636 nm while for the ionized zinc (ZnII) the lines were observed at 480 nm and 589 nm. These results are in agreement with the experimental results published in Yang et al. (2011), Ono and Iizuka (2011), Saji et al. (2006), Redwing et al. (2006) and ATOMIC DATABASE (xxxx). The intensities of the emission lines are dependent on Ar/H ratio. The intensity of the emission lines of 471, and 480 nm increased with the increase in the hydrogen gas ratio. The blue light emission from neutral Zn produced in the plasma is one of the most important factors for the deposition of ZnO nanorods. The weak blue light emission indicates no ZnO nanorods detected on the substrate (Ono and Iizuka, 2011).

The X-ray diffraction (XRD) analysis of the deposited ZnO thin film was performed using XPert Pro system with Cu-Kα radiation (λ = 1.54060 Å), operated at 40 kV and 40 mA. Fig. 4 shows a typical XRD pattern of the ZnO nano crystals on the glass substrate for three different gas ratios of hydrogen to argon. The three gas ratios are (3:1) Torr for S_1, (5:2) Torr for S_2, and (6:2) Torr for S_3 with a total ambient gas pressure of 4, 7 and 8 Torr respectively. The X-ray diffraction patterns of the crystalline ZnO thin film shown in Fig. 4 indicate that the film has polycrystalline nature. They also reveal the existence of a hexagonal wurtzite structure.

In Fig. 4, XRD diffraction peaks at 31.6, 34.4, 47.9, and 57.2 correspond to (100), (002), (102) and (110) plans respectively.

The XRD patterns consist of a (100) main peak. The full width at half maximum (FWHM) of (100) peak was 0.138 degree for the crystalline ZnO thin film. It was also noticed that the orientation (102) is another main orientation. The other orientations such as (002), and (110) are also present

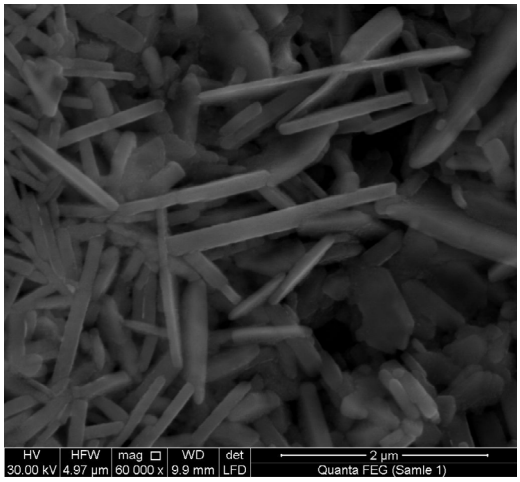

(a)

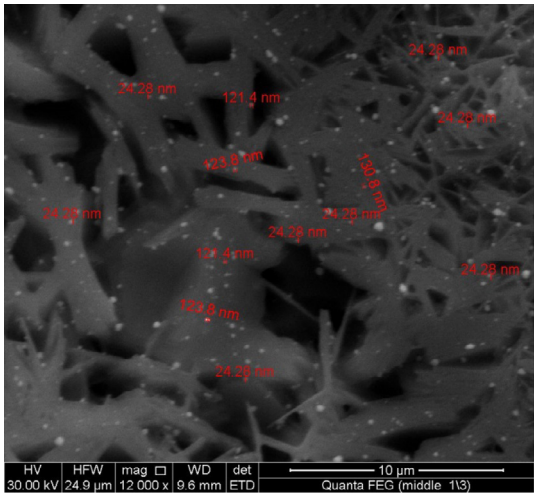

(b)

Figure 7 SEM images of ZnO nanostructure (a) partial gas pressure ratio of hydrogen and argon (3:1), (b) partial gas pressure ratio of hydrogen and argon is (5:2).

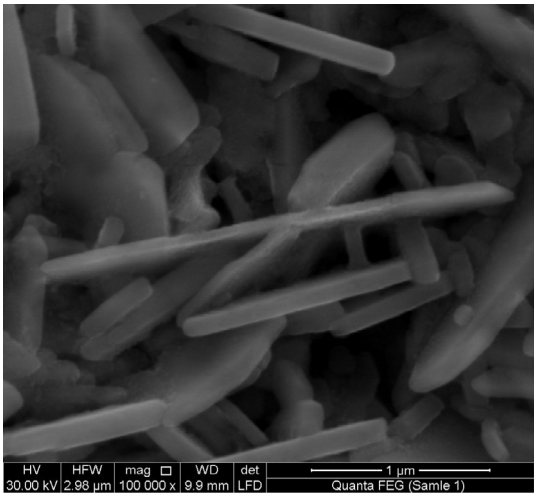

(a)

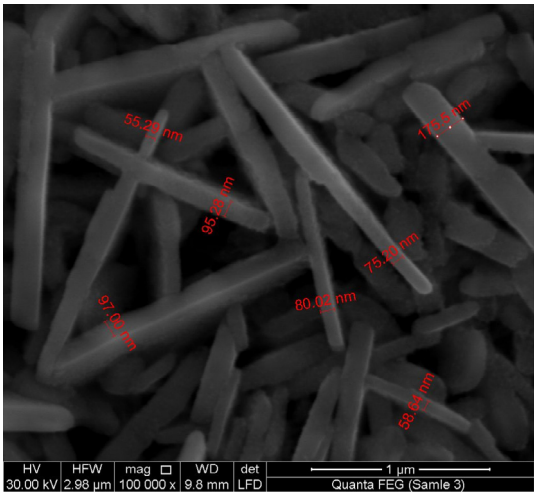

(b)

Figure 8 SEM images of ZnO nanostructure (a) partial gas pressure ratio of hydrogen and argon is (3:1), (b) partial gas pressure ratio of hydrogen and argon is (6:2).

but with relatively low intensities which indicate that samples S_1, S_2, and S_3 are composed of pure ZnO nanorods as agreed with other studies (Kang et al., 2009; Fan, 2009; Seomoon et al., 2011). The sharp diffraction peaks confirm the high crystallinity of the synthesized nanoparticles.

The grain size of the crystallites was calculated using the well-known standard Scherer's formula (Caglar et al., 2006),

$$g = \frac{0.9\lambda}{\beta \cos\theta} \tag{1}$$

where g is the grain size of crystallite, ($\lambda = 1.5060$ Å) the wavelength of X-ray used, β the broadening of diffraction line measured at half its maximum intensity in radians and (θ) is the angle of diffraction in degree.

The grain sizes are calculated using 2θ, d-value and the full width at half maximum (FWHM) of zinc oxide nanoparticles for samples S_1, S_2 and S_3 prepared at a gas mixture of hydrogen and argon and are given in Table 2a–c.

In general, the change in FWHM reflects the change in the grain size crystallites. In other words, the increase in FWHM corresponds to the decrease in the grain size (Fu et al., 2004). The calculated values of the grain size are listed in Table 2a–c. The average grain size for sample S_1 was 60 nm while for samples S_2 and S_3 were 61 nm, and 78 nm respectively. The FWHM has decreased a little with the increase of hydrogen–argon gas pressure ratio (Fu et al., 2004). The obtained data in Table 2 show the dependence of the crystal structure of the samples on the total ambient gas pressure. Table 2a–c reveals that, the main plane generated with a mixture of total pressure 7–8 Torr is (1 0 0). On the other hand at total pressure 4 Torr the (0 0 2) plane is dominant.

4. Optical properties of the crystalline zinc oxide thin film

The absorption coefficient α of the ZnO film was determined from transmittance measurements. The energy gap (E_g) is estimated by assuming a direct transition between valance and conduction bands using the following (Caglar et al., 2006).

$$\alpha h\nu = k(h\nu - E_g)^{1/2} \quad (2)$$

where α is the absorption coefficient, k is a constant, and E_g is determined by extrapolating the straight-line portion of the spectrum to $\alpha h\nu = 0$.

Fig. 5 shows the relation between hν and $(\alpha h\nu)^2$ at different partial pressure gas ratios of hydrogen:argon, (a) 3 Torr:1 Torr and (b) 5 Torr: 2 Torr. The calculated E_g in both cases are 2.95 and 3.1 eV respectively. It is clear that the value of E_g shows a slight dependence on the gas ratio.

5. Scanning electron microscopy (SEM)

The morphology of the so-obtained crystalline zinc oxide thin films was studied with scanning electron microscopy (SEM). Figs. 6–8 show high resolution SEM images of samples S_1, S_2, and S_3 respectively. The SEM images were taken using scanning electron microscope (SEM) model Quanta FEG 250 attached with the EDX unit, at an accelerating voltage of 200 V–30 kV, and magnification of 14× up to 1,000,000×.

It is clear from the SEM images that the morphology of the thin films depends on the gas mixture ratio. The change in the gas mixture ratio produces nanowires and nanorods with different shapes, lengths and widths. The following findings could be extracted from the SEM images:

1. There is a linear coupling of nanorods with nanowires having a total length in the order of ~2 μm as shown in Fig. 6.
2. Different structures of nanorods with the length of 1 μm mixed with a nanoparticle of 63 nm average diameter are as shown in Fig. 7.
3. The average diameter of the nanorods is 70 nm as shown in Fig. 8.

6. Conclusion

Transparent ZnO crystalline thin films have been successfully prepared by the plasma enhanced chemical vapor deposition (PECVD) technique onto the glass substrate at low temperatures. A gas mixture of hydrogen and argon was used as a carrier gas at stable low pressure plasma induced by microwave inside cylindrical symmetric waveguide. The crystal structure and orientation of the zinc oxide thin film were investigated by XRD. The XRD pattern consists of a (100) main peak. The full width at half maximum (FWHM) of the (100) peak was 0.138 2θ for the crystalline ZnO thin film. Another major orientation present at (102) along with lower intensity orientations is observed. This indicated that samples S_1, S_2, and S_3 are composed of pure ZnO with a hexagonal structure. The sharp diffraction peaks confirm the high crystallinity of the synthesized nanoparticles (Fan, 2009). The energy band gap, E_g, was calculated according to Eq. (2). It is clear that the value of E_g shows a slight dependence on the gas ratio. The value of E_g increases with the increase of the gas mixture ratio.

The successful synthesis of ZnO by PECVD could provide a crystalline zinc oxide thin film with a high transmittance (95%), wide band gap value of 3.37 eV, different shapes and grain sizes (24–70 nm) that depend on the ambient gas mixture ratio. The crystalline zinc oxide thin film could be used in many applications such as solar cells, gas sensors, and surface acoustic devices. The electrical properties of the deposited zinc oxide thin films need further investigation.

Acknowledgement

The authors are very grateful to the International Bureau KFA, Julich, Germany, for supporting the laboratory with the instrumentation used in carrying out this study.

References

Ashida, A., Fujita, A., Shim, Y.G., Wakita, K., Nakahira, A., 2008. ZnO thin films epitaxially grown by electrochemical deposition method with constant current. Thin Solid Films 517, 1461–1464.

Bashir, A., Wobkenberg, P.H., Smith, J., Ball, J.M., Adamopoulos, G., Bradley, D.D.C., Anthopoulos, T.D., 2009. High-performance zinc oxide transistors and circuits fabricated by spray pyrolysis in ambient atmosphere. Adv. Mater. 21, 2226–2231.

Caglar, M., Caglar, Y., Ilican, S., 2006. The determination of the thickness and optical constants of the ZnO crystalline thin film by using envelope method. J. Optoelectron. Adv. Mater. 8 (4), 1410–1413.

Chang, P.C., Fan, Z.Y., Wang, D.W., Tseng, W.Y., Chiou, W.A., Hong, J., Lu, J.G., 2004. ZnO nanowires synthesized by vapor trapping CVD method. Chem. Mater. 16 (24), 5133–5137.

Craciun, V., Elders, J., Gardeniers, J.G.E., Geretovsky, J., Boyd, I.W., 1995. Growth of ZnO thin films on GaAs by pulsed laser deposition. Thin Solid Films 259.

Fan, D.H., 2009. Synthesis of ZnO hollow spherical structures with different surface-to-volume ratios. Appl. Phys. A 96, 655–660.

Fu, En-Gang, Zhuang, D., Zhang, G., Ming, Z., Yang, W., Liu, J., 2004. Properties of transparent conductive ZnO Al thin films prepared by magnetron sputtering. Microelectron. J. 35, 383–387.

Gao, P.X., Wang, Z.L., 2002. Self-assembled nanowire-nanoribbon junction arrays of ZnO. J. Phys. Chem. 106 (49), 12653–12658.

Irzh, A., Genish, I., Klein, L., Solovyov, L.A., Gedanken, A., 2010. Synthesis of Zno and Zn nanoparticles in microwave plasma and their deposition on glass slides. Langmuir 26 (8), 5976–5984.

Ismail, L.Z., Youssif, M.I., Abdel Moneim, H.M., 2002. Microwave plasma oxidation technique for HoBa2Cu3O7-x ceramic superconductor. Mater. Chem. Phys. 76, 69–74.

Ismail, L.Z., Youssif, M.I., Abdel Moneim, H.M., 2003. The effect of oxygen plasma generated by different microwave modes on NdBa2Cu3 + δ superconductor: structure and IR studies. J. Phys. Chem. Solids 64, 1405–1411.

Ismail, L.Z., EL-Magd, A.A., 1992. Pressure dependence of the electrical potential and electron temperature plasma. IEEE Trans. Plasma Sci. 20 (2).

Kang, S., Shin, T.I., Kim, S.W., Yoon, D.H., 2009. Homojunction of single-crystalline ZnO nanowire/nanowall network on c-Al_2O_3 substrate formed by thermal vapor phase epitaxy method. Jpn. J. Appl. Phys. 48, 095502-1–095502-4.

Masuda, Y., Kato, K., 2009. Aqueous synthesis of ZnO rod arrays for molecular sensor. Cryst. Growth 311, 3083–3088.

Newton, M.C., Warburton, P.A.W., 2007. ZnO tetrapod nanocrystals. Mater. Today 10 (5).

NIST ATOMIC DATABASE.

H. Ono, S. Iizuka, Two-step formation of ZnO nanowires using energy-controlled hollow-type magnetron RF Plasma, 30th ICPIG, August 28th–September 2nd, Belfast Northern Ireland, UK, 2011.

Redwing, R., Budi, W.S., Abdulmadjid, S.N., Pardede, M., 2006. Film analysis employing sub target effect using 355 nm Nd-YAG laser–induced plasma at low pressure. Spectrochim. Acta B 61, 1285–1293.

Saji, K.J., Joshy, V., Jayarj, M.K., 2006. Optical emission spectroscopic studies on laser ablated zinc oxide plasma. J. Appl. Phys. 100, 043302-1–043302-5.

Seomoon, K., Lee, J., Jang, P., Jung, C., Kim, K., 2011. Synthesis and characterization of ZnO thin films deposited via PE-MOCVD. Curr. Appl. Phys., 1–4.

Singh, S., Kumar, R., Ganguli, T., Srinivasa, R.S., Major, S.S., 2008. High optical quality ZnO epilayers grown on sapphire substrates by reactive magnetron sputtering of zinc target. J. Cryst. Growth 310, 4640–4646.

Tang, L., Zhou, B., Tian, Y., Sun, F., Li, Y., Wang, Z., 2008. Synthesis and surface hydrophobic functionalization of ZnO nanocrystals via a facile one-step solution method. Chem. Eng. J. 139, 642–648.

Yang, H., i-Seung Lee, J., Bae, S., Hwang, J.H., 2009. Density-controlled growth of ZnO nanorods using ZnO nanocrystals-embedded polymer composite. Curr. Appl. Phys. 9, 797–801.

Yang, R., Zheng, J., Li, W., Qu, J., Zhang, X., Li, X., 2011. Low-temperature growth of ZnO nanostructures by oxygen plasma oxidation of $ZnCl_2$. Mater. Chem. Phys. 129, 693–695.

Zhang, H., Yang, D., Ji, Y., Ma, X., Xu, J., Que, D., 2004. Low temperature synthesis flowerlike ZnO nanostructure by cetyltrimethylammonium bromide-assisted hydrothermal process. J. Phys. Chem. 108 (13).